

SPECTROSCOPIC ABUNDANCES IN THE OPEN CLUSTER, NGC 6819

DONALD B. LEE-BROWN AND BARBARA J. ANTHONY-TWAROG¹

Department of Physics and Astronomy, University of Kansas
Lawrence, KS 66045-7582, USA
donald@ku.edu, bjat@ku.edu

CONSTANTINE P. DELIYANNIS¹

Department of Astronomy, Indiana University
Bloomington, IN 47405-7105, USA

EVAN RICH²

Department of Physics and Astronomy, University of Kansas
Lawrence, KS 66045-7582, USA

AND

BRUCE A. TWAROG

Department of Physics and Astronomy, University of Kansas
Lawrence, KS 66045-7582, USA

Accepted for publication in the Astronomical Journal 01/16/15

ABSTRACT

High-dispersion spectra of 333 stars in the open cluster NGC 6819, obtained using the HYDRA spectrograph on the WIYN 3.5m telescope, have been analyzed to determine the abundances of iron and other metals from lines in the 400 Å region surrounding the Li 6708 Å line. Our spectra, with signal-to-noise per pixel (SNR) ranging from 60 to 300, span the luminosity range from the tip of the red giant branch to a point two magnitudes below the top of the cluster turnoff. We derive radial and rotational velocities for all stars, as well as [Fe/H] based on 17 iron lines, [Ca/H], [Si/H], and [Ni/H] in the 247 most probable, single members of the cluster. Input T_{eff} estimates for model atmosphere analysis are provided by $(B - V)$ colors merged from several sources, with individual reddening corrections applied to each star relative to a cluster mean of $E(B - V) = 0.16$. Extensive use is made of ROBOSPECT, an automatic equivalent width measurement program; its effectiveness on large spectroscopic samples is discussed. From the sample of likely single members, $[Fe/H] = -0.03 \pm 0.06$, where the error describes the median absolute deviation about the sample median value, leading to internal precision for the cluster below 0.01 dex. The final uncertainty in the cluster abundance is therefore dominated by external systematics due to the temperature scale, surface gravity, and microturbulent velocity, leading to $[Fe/H] = -0.02 \pm 0.02$ for a sub-sample restricted to main sequence and turnoff stars. This result is consistent with our recent intermediate-band photometric determination of a slightly subsolar abundance for this cluster. [Ca/Fe], [Si/Fe], and [Ni/Fe] are determined to be solar within the uncertainties. NGC 6819 has an abundance distribution typical of solar metallicity thin disk stars in the solar neighborhood.

Subject headings: open clusters and associations : individual (NGC 6819), stars : abundances

1. INTRODUCTION

NGC 6819 is an old (2.3 Gyr) open cluster whose fundamental properties have garnered increasing attention in recent years. As detailed in Anthony-Twarog, Deliyannis, & Twarog (2014), (hereinafter Paper I), its age places it in a sparsely populated range of open cluster ages, making it an invaluable testbed for stellar models of stars just above the Sun's mass. It was chosen as a key

cluster in our program to map the evolution of Li among stars of varying mass as they evolve from the main sequence to the tip of the giant branch and beyond. Delineation of such a map requires reliable estimates of stellar temperature, luminosity, and metallicity, especially iron, and, indirectly, the cluster reddening, distance modulus and age.

Data on individual cluster stars and the surrounding field have expanded due to the cluster's location in the *Kepler* field, bringing the added potential for asteroseismic insight into the structure of individual stars in a variety of evolutionary states (Gilliland et al. 2010). Reliable radial velocities are available for a large sample of stars extending well below the cluster turnoff (Hole et al. 2009) (hereinafter H09) and improved proper-motion memberships by Platais et al. (2013) (hereinafter PL)

WIYN Open Cluster Study LXV

¹ Visiting Astronomer, Kitt Peak National Observatory, National Optical Astronomy Observatory, which is operated by the Association of Universities for Research in Astronomy (AURA) under cooperative agreement with the National Science Foundation.

² Current affiliation: Department of Physics & Astronomy, University of Oklahoma, Norman, OK 73019, USA

have supplanted the older data of Sanders (1972). Comprehensive broad-band (Rosvick & VandenBerg 1998; Kalirai et al. 2001; Yang et al. 2013) and intermediate-band (Paper I) photometric surveys allow precise determination of each star’s position in the color-magnitude diagram (CMD), while definitively demonstrating (PL, Paper I) that the cluster suffers from variable foreground reddening with a range of $\Delta E(B - V) = 0.06$ mag, not surprising given the cluster’s galactic coordinates ($l, b = 74^\circ, +8^\circ$) and a distance of 2.4 kpc from the Sun. Until recently, the weakest link in the discussion of the properties of the cluster and its stars has been the cluster metallicity. As detailed in Paper I, metallicity estimation from cluster members has been plagued by small number statistics often coupled with incorrect assumptions of uniform and/or anomalously high reddening, leading to a consensus view that NGC 6819 was metal-rich, with $[\text{Fe}/\text{H}] \sim +0.1$. Precise intermediate-band photometry on the extended Stromgren system (Paper I) strongly contradicts this claim, producing $[\text{Fe}/\text{H}] = -0.06 \pm 0.04$ from 278 single, unevolved F stars.

Although a fuller discussion of the Lithium abundances for our large sample in NGC 6819 is in preparation (Deliyannis, Twarog, Lee-Brown & Anthony-Twarog 2015), one preliminary result - the identification of a Li-rich giant star - was reported in Anthony-Twarog et al. (2013). We employ a combination of spectral synthesis and curve-of-growth analysis to convert measured equivalent widths for the Li line at 6707.8 Å to Lithium abundances, $A(\text{Li})$. Our curve-of-growth analysis method depends on subtracting an estimated contribution by an iron line at 6707.4 Å from the equivalent width, for which accurate temperature and iron abundance information is required. Given the criticality of a precise estimate of the stellar Fe abundance for derivation of Li from spectroscopy, especially among the giants, it was decided that all measurable lines within the wavelength range of our HYDRA high dispersion spectra of the Li 6708 Å region would be used to estimate the cluster metallicity for Fe and other elements. In addition to testing the photometric abundance, following the pattern laid out in our earlier investigations of the open clusters NGC 3680 (Anthony-Twarog et al. 2009) and NGC 6253 (Anthony-Twarog et al. 2010), such data could reveal the effects of stellar evolution on surface abundances through comparison of the red giants to the turnoff stars, while pinpointing the place of the cluster within the global context of galactic chemical evolution.

The layout of the paper is as follows. Sec. 2 details the spectroscopic observations and reduction of images to uniformly wavelength-calibrated and continuum-fitted spectra. Sec. 3 explains the collation of radial-velocity, photometric, proper-motion, and reddening data used to define the crucial temperatures, surface gravities, and microturbulent velocities for single-star cluster members that, together with appropriate model atmospheres, translate the spectroscopic measures to abundances. Sec. 4 supplies a detailed examination of ROBOSPECT, an automated line-measurement program used for this study which makes internally consistent and rapid abundance estimation for hundreds of stars feasible. Sec. 5 presents the abundance results for individual stars and the cluster as a whole, delineating the impact of the parametric un-

certainties on our final results, and places the data within the context of both stellar and galactic evolution. Sec. 6 summarizes our conclusions.

2. SPECTROSCOPIC DATA

Spectroscopic data were obtained for target stars in NGC 6819 using the WIYN 3.5-meter telescope³ and HYDRA multi-object spectrograph over 13 nights from September and October 2010, June 2011 and February 2013. The positions of the target stars within the cluster ($V, B - V$) CMD are shown in Figure 1. Six configurations were designed to position fibers on a total of 333 stars. The brightest configurations include stars near $V \sim 11$, while the fainter configurations reach to $V \sim 16.5$. Individual exposures ranged from 10 to 90 minutes, with accumulated totals of 2.5 to 4.5 hours for stars in the brightest configurations, 10 to 13 hours for the configuration with stars of intermediate brightness, and over 14 hours total for the faintest configurations. Our spectra cover a wavelength range ~ 400 Å wide centered on 6650 Å, with dispersion of 0.2 Å per pixel. Examination of Thorium-Argon lamp spectra indicates that the line resolution comprises 2.5 pixels, yielding a spectral resolution over 13,000.

The data were processed using standard reduction routines in IRAF⁴. These routines included, in order of application, bias subtraction, division by the averaged flat field, dispersion correction through interpolation of the comparison spectra, throughput correction for individual fibers using daytime sky exposures in the same configuration, and continuum normalization. After flat field division and before the dispersion correction, the long-exposure program images were cleaned of cosmic rays using “L. A. Cosmic”⁵ (van Dokkum 2001). Real-time sky subtraction was accomplished by using the dozens of fibers not assigned to stars and exposed to the sky for each integration. Composite spectra for each of the six configurations were constructed by additive combination.

The signal-to-noise ratio per pixel (SNR) may be estimated two ways: first, by direct inspection of the spectra within IRAF’s SPLOT utility, using mean values and r.m.s. scatter from a relatively line-free region or, second, by construction from output files of the ROBOSPECT software suite. We found the ROBOSPECT values to be entirely consistent with hand-measured SNR values and quote the ROBOSPECT-derived values in Table 1, computed from the relatively line-free 6680-6694 Å region. SNR estimates reflect the statistics characterizing the summed composite spectra.

3. STELLAR PROPERTIES

3.1. Radial Velocities and Proper Motions

An initial spectroscopic sample of probable cluster members was taken from the valuable radial-velocity

³ The WIYN Observatory is a joint facility of the University of Wisconsin-Madison, Indiana University, Yale University, and the National Optical Astronomy Observatory.

⁴ IRAF is distributed by the National Optical Astronomy Observatory, which is operated by the Association of Universities for Research in Astronomy, Inc., under cooperative agreement with the National Science Foundation.

⁵ <http://www.astro.yale.edu/dokkum/lacosmic/>, an IRAF script developed by P. van Dokkum (van Dokkum 2001); spectroscopic version.

survey of NGC 6819 by H09. All stars brighter than $V \sim 16.75$ with radial-velocity membership probabilities greater than 50% were identified as candidates for the present study. Stars classed as double-lined spectroscopic binaries were eliminated; single-lined systems were retained since the existence of the companion would have minimal impact on line measurement. Stars were not eliminated based upon their position in the CMD to avoid biasing the sample against stars undergoing anomalous evolution.

Individual stellar radial velocities were derived from each summed composite spectrum utilizing the Fourier-transform, cross-correlation facility FXCOR in IRAF. In this utility, program stars are compared to stellar templates of similar effective temperature (T_{eff}) over the wavelength range from 6575 Å to 6790 Å, as well as a narrower region in the vicinity of H α alone. Typical uncertainties in the individual radial velocities were estimated at 1.15 km/sec. The FXCOR utility also provides measures of the line widths within each spectrum, from which rotational velocities may be inferred. Observations of a pair of radial-velocity standards were obtained during each run and processed using the same procedure applicable to the cluster. Comparison of the velocity zero-points using standard values from the General Catalog of Radial Velocities (Wilson 1953) allowed transformation of the cluster data to the standard system, within the uncertainties of the measurements.

As a first check on our spectroscopic data, we can compare our measured radial velocities with those of H09 to identify discrepant stars or long-term variables. Eliminating 29 stars classed as spectroscopic binary members of NGC 6819, the remaining 304 single stars have a mean radial velocity of 2.65 ± 1.36 (s.d.) km/sec. The same sample from H09 has a mean velocity of 2.38 ± 0.99 (s.d.) km/sec. The dispersion in the residuals between these samples is 1.06 km/sec; the predicted dispersion from the quoted errors for each star is 1.19 km/sec. The residuals for only three stars (WOCS 1007, 2016 and 56018) fall more than three sigma from the mean; one of these, WOCS 2016, has unusually broad lines (presumably due to high rotational velocity) which leads to a larger than average uncertainty in the final radial-velocity estimate. By contrast, the sample of 29 spectroscopic binaries has a mean cluster velocity of 3.45 km/sec and a dispersion of 9.8 km/sec; the same stars from H09 exhibit a dispersion of 9.78 km/sec. We conclude that all single star members as classified by H09 are confirmed as such by our data. Table 1 contains the derived mean radial and estimated rotational velocities for each star in our survey.

At the start of our program, the only NGC 6819 proper-motion study available was that of Sanders (1972), which proved inadequate for reliable identification of probable members, particularly at the fainter limit of interest. Fortunately, the comprehensive survey by PL covers the appropriate range in both area and depth, generating probabilities for all stars in our sample except one. Of 332 stars selected via radial velocity, 59 have proper-motion membership probabilities below 50%, 43 of which are in single digits. The PL values for individual stars may be found in Table 1. The different stellar categories are identified in the CMD, Fig. 1.

3.2. Effective Temperature, Surface Gravity, and Microturbulent Velocity

In keeping with our approach to spectroscopic abundance determination for previous clusters in this program, our default scheme for determining model atmosphere input temperatures is based upon photometric color, specifically $B - V$. Four sources of broad-band BV data exist. As a first step, we merged the CCD photometry presented by H09 as PHOT98 and PHOT03. From 923 stars brighter than $V = 16.7$, excluding 5 stars with absolute residuals greater than 0.10 mag, the mean offsets, in the sense (PHOT98 - PHOT03), in V and $B - V$ are -0.005 ± 0.022 and $+0.003 \pm 0.022$, respectively. While the dispersion in both sets of residuals was satisfactory, further analysis revealed that a large fraction of the scatter in V is the result of a nonlinear radial gradient among the residuals, reaching $\Delta V = -0.05$ mag for stars near the core of the cluster but $+0.01$ for stars in the outer regions of the frame. Milliman et al.

(2014) have independently discovered the same effect in a comparison between the VI photometry of Yang et al. (2013) and PHOT03, implying that the primary source of the trend in the current comparison must lie with the PHOT03 database. Additional evidence in support of this conclusion comes from a direct comparison between the V magnitudes from Yang et al. (2013) and the intermediate-band data from Paper I where the residuals do not exhibit a radial dependence. More important from our perspective is the absence of a radial trend among the residuals in $B - V$ between the two samples, PHOT98 and PHOT03. Application of a small color term, $(B - V)_{03} = 0.986(B - V)_{98} + 0.006$, reduces the scatter in the residuals to ± 0.021 mag. The PHOT98 $B - V$ data were converted to the PHOT03 system and averaged for stars common to both samples.

Next, the composite H09 data were transformed to our adopted standard of Rosvick & Vandenberg (1998). From 470 stars with V brighter than 16.5 common to the two datasets, removing 10 stars with residuals in $B - V$ greater than 0.05 mag, the mean residual, in the sense (RV-H09), is $+0.006 \pm 0.014$ mag. A weak color dependence among the residuals was found, $(B - V)_{RV} = 1.007(B - V)_{H09}$, and applied prior to the merger of the two databases, eliminating the small zero-point offset.

Finally, a transformation was derived between the $B - V$ indices of Kalirai et al. (2001) and the previously merged $B - V$ data on the Rosvick & Vandenberg (1998) system; comparisons of the V mags of Rosvick & Vandenberg (1998) and Kalirai et al. (2001) have already been discussed in Paper I.

Eliminating 11 stars with absolute residuals greater than 0.1 mag and applying a small color term, $(B - V)_{RV} = 1.025(B - V)_{KA} - 0.018$, 846 stars brighter than $V = 16.5$ exhibit a mean residual in $B - V$ of 0.000 ± 0.018 mag.

All stars with absolute residuals greater than 0.05 mag were individually checked. If $B - V$ estimates were available from more than two sources and one source was clearly the origin of the discrepancy, that value was dropped. If only two sources of $B - V$ existed, an independent check on the predicted $B - V$ was attempted using the published $V - I$ data of Yang et al. (2013). In cases where no resolution of the discrepancy was possible,

the averaged value from all sources was retained. Averaged $B - V$ indices from the four transformed primary data sets are given in Table 1 along with the number of sources and each star’s estimated individual reddening correction.

As noted earlier, PL identified and mapped variable reddening across the field of NGC 6819, a result confirmed in Paper I. We used the map of individual reddening values derived by PL to estimate by spatial interpolation the degree of reddening affecting each of the stars in our spectroscopic sample. Individual reddening estimates, with a range of ± 0.033 about our adopted mean value of $E(B - V) = 0.16$, were applied to each star’s $(B - V)$ color. A temperature for each star based on its dereddened $(B - V)$ color was then derived using two primary color-temperature calibrations.

For dwarfs, we continue to use a calibration (Deliyannis, Steinhauer & Jeffries 2002) consistent with previous spectroscopic studies by this group, namely:

$$T_{eff} = 8575 - 5222.7(B - V)_0 + 1380.92(B - V)_0^2 + 701.7(B - V)_0[[\text{Fe}/\text{H}] - 0.15] \text{ K.}$$

For giants, the T_{eff} -color- $[\text{Fe}/\text{H}]$ calibration of Ramírez & Meléndez (2005) was used. We note that for 13 stars, it was possible to obtain temperatures from both color-temperature calibrations. Temperatures derived from the Deliyannis, Steinhauer & Jeffries (2002) calibration are 41 ± 6 K higher for these mostly subgiant stars.

Surface gravity estimates ($\log g$) were obtained by direct comparison of V magnitudes and $B - V$ colors for our sample of 333 stars to isochrones from the Y^2 compilation (Demarque et al. 2004), constructed for a scaled solar composition with $[\text{Fe}/\text{H}] = -0.06$ and an age of 2.3 Gyr, essentially the same as the comparison presented in Paper I. The isochrone’s predicted magnitudes and colors were adjusted to match the cluster’s reddening, $E(B - V) = 0.16$ and apparent distance modulus, 12.40. For stars that appear to be blue stragglers, surface gravities were estimated by comparing photometric information to a grid of younger isochrones of similar composition.

We are fortunate to have independent confirmation of the $\log g$ values for the giant branch stars, thanks to their status as *Kepler* objects of interest. We compared $\log g$ values from our isochrone match to $\log g$ values inferred using asteroseismology from *Kepler* data, as presented by Basu et al. (2011) for 21 giants. The seismological gravities are in remarkable agreement with the isochrone-inferred gravities, differing by an insignificant amount, -0.02 ± 0.04 where the listed error is the standard deviation.

Input estimates for the microturbulent velocity parameter were constructed using various prescriptions. For dwarfs within appropriate limits of T_{eff} and $\log g$, the formula of Edvardsson et al. (1993) was used; a similar formulation by Ramírez, Allende Prieto, & Lambert (2013) extends to slightly lower temperatures and gravities and was used for some stars. For giants, a gravity-dependent formula, $V_t = 2.0 - 0.2 \log g$, was used. For some subgiants and candidate blue stragglers, no suitable formula for V_t was found other than the purely gravity-dependent expression employed by the SDSS collaboration in their DR10 data release and discussion of the abundance analysis pipeline for APOGEE spectra (Ahn et al. 2014).

4. SPECTROSCOPIC PROCESSING WITH ROBOSPECT

With the expansion in spectroscopic samples from a few dozen stars in previous cluster work (Anthony-Twarog et al. 2009, 2010) to a few hundred in this and future analyses, manual measurement of equivalent widths (EW) for individual lines is now prohibitive. To overcome this obstacle, the automated line-measuring program, ROBOSPECT (Waters & Hollek 2013) (hereinafter WH), has been utilized. For full details, the reader is referred to WH; a brief outline of the program operation and our procedure is provided here. ROBOSPECT measures EW by first determining the continuum level and constructing a noise profile across the wavelength range of interest using an iterative process. With the initial continuum and noise levels established, spectral lines are tagged at locations specified by a user-supplied line list, and other potential lines are automatically identified based on significant deviations of the local spectrum from the continuum. For the automatic line identification, the significance threshold is user-specified and based on the current noise solution. After lines are identified through these two processes, they are subtracted from the spectrum and the continuum process is repeated and the noise level refined. Through multiple iterations, the best-fit continuum and individual line solutions are reached. For this study, each spectrum was individually corrected in ROBOSPECT for radial velocity and run through 25 iterations of continuum fitting and line estimation using a gaussian line profile with three-sigma automatic line identification and no least-squares line deblending. All other parameters for the program were set to default values.

An issue of obvious concern with any automated procedure is the potential for unreliable EW due to low SNR spectra, line blending, or inaccurate radial-velocity correction. With interactive measurement, such issues can be flagged and corrected or eliminated but, with ROBOSPECT, flawed EW measures propagate to followup steps in the abundance determination process, potentially distorting the final results. It is expected that the uncertainty in EW will increase with decreasing SNR, potentially reaching a level where the subsequent uncertainty in a star’s calculated abundance renders it useless. Similarly, we can expect the EW uncertainty to increase as individual lines suffer increased blending from neighboring lines. Finally, a significant error in radial velocity will cause ROBOSPECT to misidentify the wavelength of line centers. To ensure that our abundances are minimally affected by these issues, a variety of tests were conducted to determine if our line list and ROBOSPECT input parameters lead to robust results over the range in SNR and radial-velocity uncertainties spanned by our spectra. Since ROBOSPECT will be used in future analyses with similar input parameters, the level of detail supplied is somewhat greater than usual.

The line list used during this study was constructed by visually identifying relatively isolated, medium-strength (EW ~ 10 to 200 mÅ) lines in the solar spectrum, using the solar atlas of Wallace, Hinkle, & Livingston (1998) as a guide. Atomic information for each line was retrieved from the VALD database (Kupka et al. 1999). $\log gf$ values given by VALD were then modified to

force-fit abundances from ROBOSPECT analysis of solar spectrum EW to abundances in the 2010 version of the abundance analysis software, MOOG (Snedden 1973). We used day-time sky spectra, taken as part of the calibration data sets, as solar spectra for this normalization. MOOG analysis was conducted using the *abfind* driver and a solar model (Kurucz 1995) with the following atmospheric parameters: $(T_{eff}, \log g, v_t, [Fe/H]) = (5770 \text{ K}, 4.40, 1.14 \text{ km/s}, 0.00)$.

Our final line list contains 22 lines of interest (17 Fe, 3 Ni, 1 Ca, 1 Si), presented along with the relevant atomic parameters in Table 2. To minimize the impact of blending, all selected lines are at least 0.5 \AA from any line with EW greater than 5 m\AA in the solar spectrum. To further minimize measurement distortions in spectra with lower SNR, the line list input for ROBOSPECT included any significant feature within 2 \AA of a line of interest. EW for these features were disregarded during the abundance analysis. The extraneous entries were added after observing unusual amounts of scatter among the EW for lines with close neighbors, particularly at lower SNR.

To evaluate the performance of our line list and to quantify the effects of a spectrum’s SNR on EW values, we tested ROBOSPECT on 100 solar spectra, 25 each with mean SNR of 160, 130, 95 and 70. These represent typical SNR for our program stars (see Fig. 2). We note that WH include an evaluation of ROBOSPECT’s performance over a wide range of line strengths and SNR; our test results are consistent with theirs. The mean standard deviations in EW for our four test samples were 4.2, 4.7, 7.5, and 11.1 m\AA , in order of decreasing mean SNR. The uncertainty this scatter introduces into our abundance results is small relative to the uncertainty due to external systematics. At all SNRs tested, we observed no significant correlation between the mean EW of a line and its associated uncertainty. Taken together, these results indicate that our line list is robust over the range in mean EW and SNR of interest.

The effect of potential errors in the determined radial velocity on EW measurement was evaluated by artificially increasing and decreasing our best estimate of radial velocity by a flat amount in the set of 100 solar spectra. For a shift of $\pm 2.5 \text{ km/s}$, corresponding to a radial-velocity uncertainty greater than that of 99% of our program stars, the mean deviation in EW between the true and adjusted spectra was -0.7 m\AA . When the shift was increased to 5.0 km/s , corresponding to a radial-velocity uncertainty greater than that of all program stars (including the rapid rotator WOCs 2016), the mean deviation in EW increased to -3.5 m\AA . In both cases, ROBOSPECT correctly identified essentially the same number of entries from the line list as it had with the correct radial velocity. We conclude that the effect of radial-velocity error on our abundance results is negligible.

Finally, we compared ROBOSPECT results with manual EW measurements for 18 random program stars using a 10-line subset of our line list. Manually obtained EWs were measured using IRAF’s SPLIT tool. ROBOSPECT’s results largely agree with the manual values, with ROBOSPECT’s EW on average being $7.7 \pm 4.2 \text{ m\AA}$ (s.d.) lower than the manual results. We note that this consistent underestimate of EW by ROBOSPECT (or, over-estimate using SPLIT and interactive measur-

ing) is similar in solar spectra and in the spectra of program stars, and is not a function of SNR to any detectable extent, so we anticipate no effect on our abundance estimates based on differential analysis with respect to the sun.

Using our measured radial velocities and constructed line list, EWs were measured for all 333 stars in our observing program. We discarded negative EW (ROBOSPECT’s designation of emission lines) due to non-convergent fitting solutions, artifacts of cosmic ray removal, large noise spikes, or nonexistent lines in the measured spectrum. Approximately 4% of the measured lines of interest returned negative values.

5. ABUNDANCE DETERMINATIONS

Model atmospheres were constructed for each program star using the grid of Kurucz (1995) and the input T_{eff} , $\log g$ and microturbulent velocity values listed in Table 1. As a reminder, each star’s T_{eff} estimate is based on its $B - V$ color, individually dereddened based on its spatial position within the field of the cluster. For any star that is not actually a cluster member, this spatially interpolated reddening correction may be spurious; the gravity estimate based on an isochrone matched to the cluster CMD almost certainly would be as well. For suspected binaries, the color might reflect the combined light of the two stars and affect the assigned temperature. While this might not be a large issue for SB1, a few candidate SB2 were highlighted by examination of spectra: WOCs 7009, 26007, 35025, 9004 and 60021. As a conservative approach, we restricted our analysis to stars with membership probability $\geq 50\%$ (PL) and no evidence of binarity. We also excluded from our final analysis several stars with $(B - V)_0$ greater than 1.35, for which severe line-blending makes reliable measurement of equivalent widths problematic. This left us with a sample of 247 single, member stars.

Each star’s measured equivalent widths and model serve as input to the *abfind* routine of MOOG to produce individual $[A/H]$ estimates for each measured line for each star. A large volume of spectroscopic information is available for interpretation from over 7000 measured lines, with up to 17 $[Fe/H]$ values for each star. Before constructing median $[Fe/H]$ values for each star and for the sample as a whole, the following filters were applied to the individual abundance estimates: abundances based on equivalent width measurements smaller than three times the expected error in equivalent width for each star based on the star’s SNR, were not considered, nor were equivalent widths for very strong lines ($EW \geq 200 \text{ m\AA}$). We note that the consequences of using 200 or 250 m\AA as the upper limit for EW are negligible. Estimated abundances from individual lines deviant by more than 1 dex from solar were not included in the determination of $[Fe/H]$ for each star.

Figures 2 and 3 show the spread of stellar $[Fe/H]$ estimates for each star as a function of the individual spectrum SNR and unreddened $B - V$ color for each star. A few outliers with SNR below 50 are obvious, as are a few of the brightest (and coolest) stars with higher than typical abundance. Figure 3 suggests that abundances for the cooler stars appear to be slightly below the range for the stars nearer the turnoff. We further divided our

sample of 247 likely members into stars bluer than and redder than $(B - V)_0 = 0.60$ to separate out the cooler and more evolved stars and re-examined the effect of filters that precede the construction of each star’s median $[\text{Fe}/\text{H}]$ abundance. Do some of our 17 iron lines produce abundances in dwarfs that are unacceptably noisy?

By examining the effect of imposing different criteria for excluding small EW measures, we were able to highlight several iron lines, which for dwarfs, lead to biased $[\text{Fe}/\text{H}]$ values in the sense that the abundance values for these lines in dwarf stars are higher than the ensemble median value by several tenths. The reason for this is clear; if the median EW for a particular absorption line is small, imposing a 3-sigma cut will preferentially preserve stars in the sample with larger EW, and consequently larger $[\text{Fe}/\text{H}]$ values. We excluded lines in dwarfs for which imposing 3-sigma cuts changed the median EW for the line by more than 25% in comparison with a more generous 1-sigma cut. As a reminder, these lines are measured in the solar spectrum at considerably higher SNR so we may still place considerable confidence in the $\log gf$ values determined from those lines.

As this still leaves information from several thousand separate iron line measurements, we were able to further explore the consequences of these filters. A diagnostic diagram is presented in Figure 4, demonstrating the lack of a trend in the median $[\text{Fe}/\text{H}]$ for each of our 17 iron lines with wavelength, where the median value is constructed from the full sample of 247 probable-member, single stars for lines denoted by black symbols; the six lines denoted by red symbols represent measures for giant stars only. The upper panel of this figure shows the MAD (*median absolute deviation*) statistic for each line, a robust estimator of variance, constructed by comparing the $[\text{Fe}/\text{H}]$ value for each star to the median value for that particular absorption line.

For the subset of 247 single member stars bluer than $(B - V)_0 < 1.35$, the median $[\text{Fe}/\text{H}]$ value is -0.03 ± 0.06 , with abundances for the other elements that are entirely consistent with solar: -0.01 ± 0.10 , -0.01 ± 0.06 and 0.00 ± 0.06 for $[\text{Ca}/\text{H}]$, $[\text{Si}/\text{H}]$ and $[\text{Ni}/\text{H}]$, respectively. Of these 247 stars, 200 are main sequence and turnoff stars, with a median iron abundance of -0.02 ± 0.05 , while the remaining 47 cool and evolved stars show a lower $[\text{Fe}/\text{H}]$, -0.09 ± 0.05 . We note that this apparent discrepancy between giant and dwarf $[\text{Fe}/\text{H}]$ values is nearly identical to that found in NGC 3680 (Anthony-Twarog et al. 2009).

For all of these quantities, the indicated error is the MAD statistic; for a large sample size drawn from a normally distributed population, the normalized MAD statistic, $\text{MADN} = 1.48 \text{ MAD}$, approximates well the sample standard deviation, permitting an estimate of the traditional standard error of the mean through division by $(N - 1)^{1/2}$. For the sample of 247 single, probable-member stars, the MAD statistic implies a value for $\text{MADN} = 0.09$; as this statistic is a good proxy for a standard deviation, a standard error of the mean of 0.01 is implied. These values can be confirmed by computing averages, standard deviations and s.e.m. values in linear space; for these stars, the average $[\text{Fe}/\text{H}]$, computed in linear space and then converted to logarithmic values, is $-0.02^{+0.07}_{-0.13}$ (standard deviations).

Table 3 includes the median $[\text{Fe}/\text{H}]$, along with the number of iron lines included in the estimate, as well as estimates of $[\text{Ca}/\text{H}]$, $[\text{Si}/\text{H}]$ and $[\text{Ni}/\text{H}]$ for 333 stars. Stars not part of the set of 247 single, probable member stars are flagged with a note indicating non-member of binary status. The statistic that accompanies each $[\text{Fe}/\text{H}]$ estimate is the MAD. We note that the 29 stars not included in these estimates of cluster $[\text{Fe}/\text{H}]$ due to evidence of binarity, yield a similar median $[\text{Fe}/\text{H}]$ value if the suspected double-lined spectroscopic binaries are excluded. For member stars which are mostly SB1, $[\text{Fe}/\text{H}] = -0.05 \pm 0.06$, consistent with the more conservative sample that excludes binaries.

Conversions of photometric parameters to T_{eff} and V_t are fundamentally discontinuous for dwarf and giant stars; to assess the effects of parameter choices on the derived abundances, each star was reanalyzed with atmospheric parameters incremented and decremented by the following amounts: 100 K for T_{eff} , 0.25 for $\log g$ and 0.25 km/sec for V_t . A summary of the extensive results is shown in Figure 5 where once again median values and variances indicated by median absolute deviations are compiled and shown for stars in different color bins. This figure illustrates some well-known dependences of abundance determinations on stellar parameters, namely that main sequence star abundances are very sensitive to T_{eff} estimates, while evolved stars demonstrate a higher sensitivity to surface gravity and consequently to microturbulent velocity estimation schemes.

Although the discrepancy between the giant and near-turnoff samples is small, it is of value to explore modest parameter changes that could eliminate it. Reference to Figure 5 suggests that errors in $\log g$ have relatively little impact; we remind the reader that the $\log g$ values employed are consistent with values suggested by asteroseismic analyses of NGC 6819 giants. The relation used for microturbulent velocities for the evolved stars is more tenuous; a fairly modest decrement of 0.2 km/sec would raise the giant abundances to match the $[\text{Fe}/\text{H}]$ representative of the near-turnoff stars. Finally, increased abundances for both regions of the CMD would accompany higher temperatures, though a simple increment to the mean cluster reddening will have differing effects for the two classes of stars, both because of the slight color-dependence of the effect on the abundance as shown in Figure 5 and the larger increment implied for warmer stars resulting from the same higher reddening.

To define the final estimate of $[\text{Fe}/\text{H}]$ for the cluster, we default to the dwarfs, where the sensitivity to the changes in the three key input parameters (T_{eff} , V_t , $\log g$) is collectively minimized, the color range is small, and the parametric differences between the program stars and the solar reference spectra are significantly smaller than for the evolved stars. For $\log g$ and V_t we adopt 0.1 dex and 0.2 km/sec as generous estimates for the uncertainties. From Fig. 5, these translate into 0.003 and 0.008 dex, respectively. As usual, the more sensitive parameter is the temperature, tied to the $B - V$ color transformation, which has two primary components, the uncertainty in the mean cluster reddening, $E(B - V)$, and the uncertainty in the photometric zero point. From Paper I, the photometric internal and external errors combined lead to an uncertainty of 0.007 in $E(B - V)$, while the photometric merger of the four broad-band surveys above

implies an uncertainty in the $B - V$ zero-point of 0.004 mag. Combined, the $(B - V)_0$ scale is reliable to 0.008 mag. On our temperature scale, this translates to approximately 32 K or, from Fig. 5, 0.012 dex in $[\text{Fe}/\text{H}]$. Combining all three parameters, one arrives at a final external uncertainty of 0.015 dex, much larger than the internal precision of the spectroscopic average. From 200 turnoff stars, the mean $[\text{Fe}/\text{H}]$ for NGC 6819 is determined to be -0.02 ± 0.02 .

Among the prior determinations of NGC 6819's heavy element abundance, the result published by Bragaglia et al. (2001) has anchored a string of moderately super-solar values. Their study of three clump giants utilized the high dispersion ($R \sim 40,000$) spectrograph on the Galileo Italian National Telescope (TNG). Though the sample size was small, their analysis incorporated hundreds of lines, including nearly 100 iron lines, six of which were Fe II lines to permit an accurate verification of surface gravity. The reddening value of $E(B - V) = 0.14$ they adopted, however, was somewhat smaller than the mean value derived in Paper I and utilized here, $E(B - V) = 0.16$. We repeated parameter determinations for the three giants studied by Bragaglia et al. (2001), including independent determinations of spatially-dependent reddening and T_{eff} values, $\log g$ values from isochrone comparisons and microturbulent velocity values based on the surface gravities. Using the estimates of $\Delta[\text{Fe}/\text{H}]$ for each of the principal atmospheric parameters cited by Bragaglia et al. (2001), their equivalent width analysis would yield an average abundance 0.07 dex lower with our atmospheric parameters, lowering their $[\text{Fe}/\text{H}]$ for the cluster from $+0.09$ to $+0.02 \pm 0.03$, essentially solar.

6. DISCUSSION AND CONCLUSIONS

High dispersion spectra of 333 potential members of the old open cluster, NGC 6819, have been processed and analyzed. From the wavelength region near Li 6708 Å, abundances have been obtained for Fe, Ni, Ca, and Si for 247 highly probable, single-star members ranging from the tip of the giant branch to well below the top of the CMD turnoff. Using up to 17 Fe lines per star, the cluster exhibits a slightly subsolar $[\text{Fe}/\text{H}]$, a conclusion which remains unchanged if the data are sorted into evolved stars (47) or turnoff/unevolved stars (200). Due to the cumulative impact of a few thousand Fe lines, the standard error of the mean for $[\text{Fe}/\text{H}]$ tied to internal errors is below 0.01 dex, leaving the systematics of the temperature, $\log g$, and microturbulent velocity scales as the overwhelming source of uncertainty in the final cluster metallicity. Once again, thanks to the size of the

sample, we can minimize the impact of these parameters by looking only at the 200 unevolved stars since the red giant abundances have a higher degree of sensitivity to microturbulent velocity. From these stars alone, $[\text{Fe}/\text{H}] = -0.02 \pm 0.02$, where the uncertainty includes both internal and external errors. The lower metallicity compared to the commonly adopted value of $[\text{Fe}/\text{H}] = +0.09$ (Bragaglia et al. 2001) continues a trend first indicated by the intermediate-band photometry of Paper I, where precision photometry was used to derive a reliable cluster reddening and confirm the existence of variable reddening across the face of the cluster (PL), leading to subsolar $[\text{Fe}/\text{H}]$ from either m_1 or hk indices.

Within the context of Galactic evolution, NGC 6819 exhibits no features which distinguish it from a typical thin-disk population formed within the last 5 Gyrs within 1 kpc of the Sun's galactocentric distance. Its $[\text{Fe}/\text{H}]$ places it at the mean for open clusters at the solar galactocentric radius, a distribution which exhibits a scatter at only the ± 0.1 dex level (Twarog, Ashman, & Anthony-Twarog 1997). Its abundance ratios relative to Fe are all consistent with solar, a pattern which holds true within the scatter for Ni, Ca, and Si for stars with $[\text{Fe}/\text{H}] \sim 0.0$, whether they are classed as members of the thin or thick disk population (see Hinkel et al. (2014) and references therein). NGC 6819 forms a rich and ideal link for tests of stellar evolution theory midway in age between NGC 5822 (Carraro et al. 2011) and M67 (Sandquist 2004), a characteristic which will prove valuable in the analysis of the evolution of Li for intermediate mass stars evolving off the main sequence and up the giant branch.

The authors express their thanks to Imants Platais for supplying additional data to compute spatially-dependent reddening estimates in the cluster. Drs. Ryan Maderak and Jeff Cummings assisted as visiting astronomers at KPNO for runs in 2010, supplying support and advice for the spectroscopic data collection. NSF support for this project was provided to ER while he was an undergraduate at the University of Kansas through NSF grant AST-0850564 via the CSUURE REU program at San Diego State University, supervised by Eric Sandquist. NSF support for this project to BJAT, BAT and DLB through NSF grant AST-1211621, and to CPD through NSF grant AST-1211699 is gratefully acknowledged. Extensive use was made of the WEBDA⁶ database operated at the Department of Theoretical Physics and Astrophysics of the Masaryk University, the TOPCAT suite⁷ the Vienna VALD, of the MOOG suite of spectroscopic analysis software, and of ROBOSPECT software.

REFERENCES

- Ahn, C. P., Alexandroff, R., Allende Prieto, C., et al. 2014, ApJS, 211, 17
 Anthony-Twarog, B. J., Deliyannis, C. P., Twarog, B. A., Croxall, K. V., & Cummings, J. 2009, AJ, 138, 1171
 Anthony-Twarog, B. J., Deliyannis, C. P., Twarog, B. A., Cummings, J. D., & Maderak, R. M. 2010, AJ, 139, 2034
 Anthony-Twarog, B. J., Deliyannis, C. P. & Twarog, B. A. 2014, AJ, 148, 151 (Paper I)
 Anthony-Twarog, B. J., Deliyannis, C. P., Rich, E. & Twarog, B. A. 2013, ApJ, 767, 19
 Basu, S., Grundahl, F., Stello, D., et. al. 2011, ApJ, 729, L10
 Bragaglia, A., Carretta, E., Gratton, R. G., et al. 2001, AJ, 121, 327
 Carraro, G., Anthony-Twarog, B.J., Costa, E., Jones, B.J. & Twarog, B.A. 2011, AJ, 142, 127
 Deliyannis, C.P., Twarog, B.A., Lee-Brown, D.B. & Anthony-Twarog, B.J. 2015, in preparation.
 Deliyannis, C. P., Steinhauer, A., & Jeffries, R. D. 2002, ApJ, 577, L39
 Demarque, P., Woo, J. -H., Kim, Y. -C., & Yi, S. K. 2004, ApJS, 155, 667 (Y^2)

⁶ <http://www.univie.ac.at/webda>

⁷ <http://www.star.bristol.ac.uk/~mbt/topcat/>

- Edvardsson, B., Andersen, J., Gustafsson, B. et al. 1993, *A&A*, 275, 101
- Gilliland, R. L., Brown, T. M., Christensen-Dalsgaard, J., et al. 2010, *PASP*, 122, 131
- Hinkel, N. R., Timmes, F. X., Young, P. A., Pagano, M. D., & Turnbull, M. C. 2014, *AJ*, 148, 54
- Hole, K. T., Geller, A. M., Mathieu, R. D., et al. 2009, *AJ*, 138, 159 (H09)
- Kalirai, J. S., Richer, H. B., Fahlman, G. G., et al. 2001, *AJ*, 122, 266
- Kupka, F., Piskunov, N., Ryabchikova, T. A., Stempels, H. C., & Weiss, W. W. 1999, *A&A*, 138, 119
- Kurucz, R. L. 1995, in *IAU Symp. 149, The Stellar Populations of Galaxies*, ed. B. Barbuy & A. Renzini (Dordrecht: Kluwer), 225
- Milliman, K. E., Mathieu, R. D., Geller, A. M., et al. 2014, *AJ*, 148, 38
- Platais, I., Gosnell, N. M., Meibom, S., et al. 2013, *AJ*, 146, 43 (PL)
- Ramírez, I. & Meléndez, J. 2005, *ApJ*, 626, 465
- Ramírez, I., Allende Prieto, C. & Lambert, D. L. 2013, *ApJ*, 764, 78
- Rosvick, J., & Vandenberg, D. A. 1998, *AJ*, 115, 1516
- Sanders, W. L. 1972, *A&A*, 19, 155
- Sandquist, E. L. 2004, *MNRAS*, 347, 101
- Snedden, C. 1973, *ApJ*, 184, 839
- Twarog, B. A., Ashman, K., & Anthony-Twarog, B. J. 1997, *AJ*, 114, 2556
- van Dokkum, P. G. 2001, *PASP*, 113, 1420
- Wallace, L., Hinkle, K. & Livingston, W. 1998, *An atlas of the spectrum of the solar photosphere from 13,500 to 28,000 cm⁻¹ (3570 to 7405 Å)*, NSO Technical Report #98-001.
- Waters, C. Z., & Hollek, J. K. 2013, *PASP*, 125, 1164 (WH)
- Wilson, R. E., 1953, *Carnegie Inst. Washington D.C. Publ.* 601
- Yang, S.-C., Sarajedini, A., Deliyannis, C. P., et al. 2013, *ApJ*, 762, 3

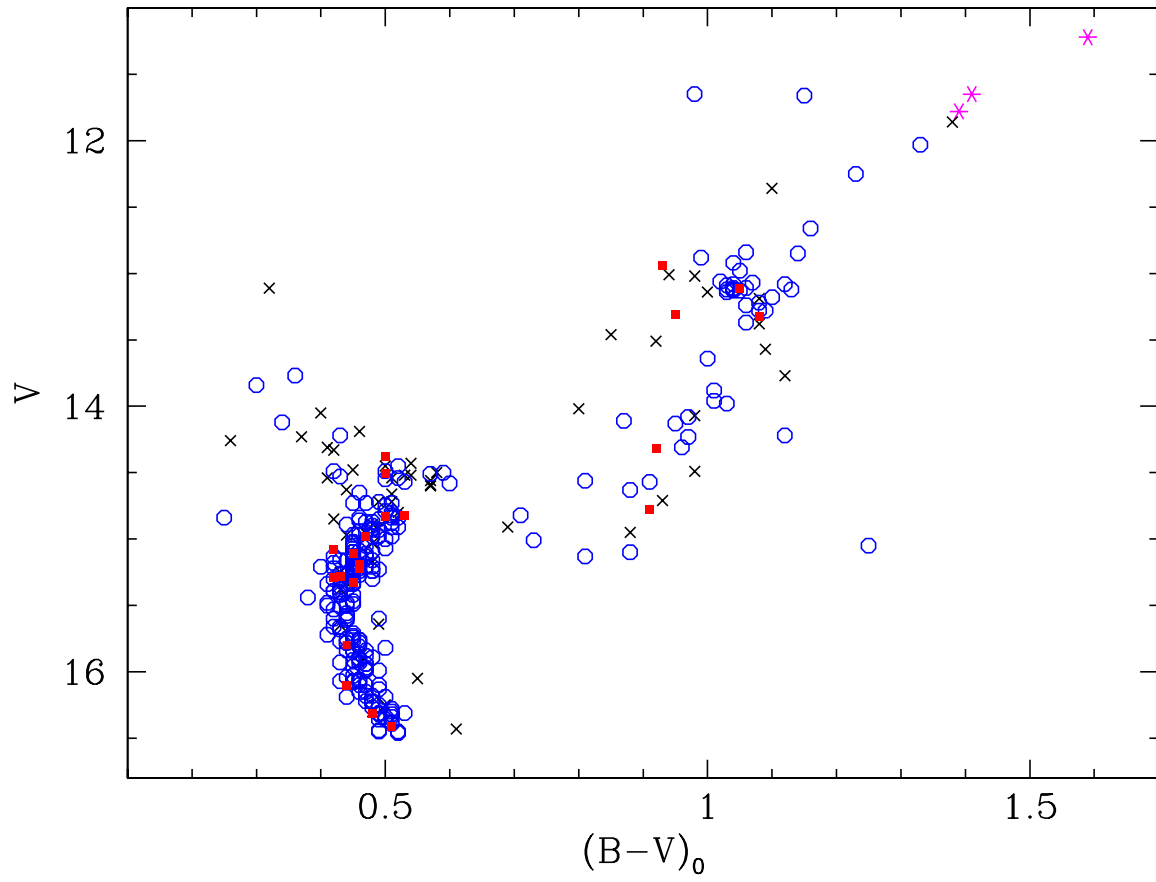


FIG. 1.— Color-magnitude diagram of spectroscopic sample. Blue open circles denote single, probable member stars. The few large magenta asterisks mark stars with very cool colors, while black crosses mark probable nonmembers and red filled squares denote probable member spectroscopic binaries.

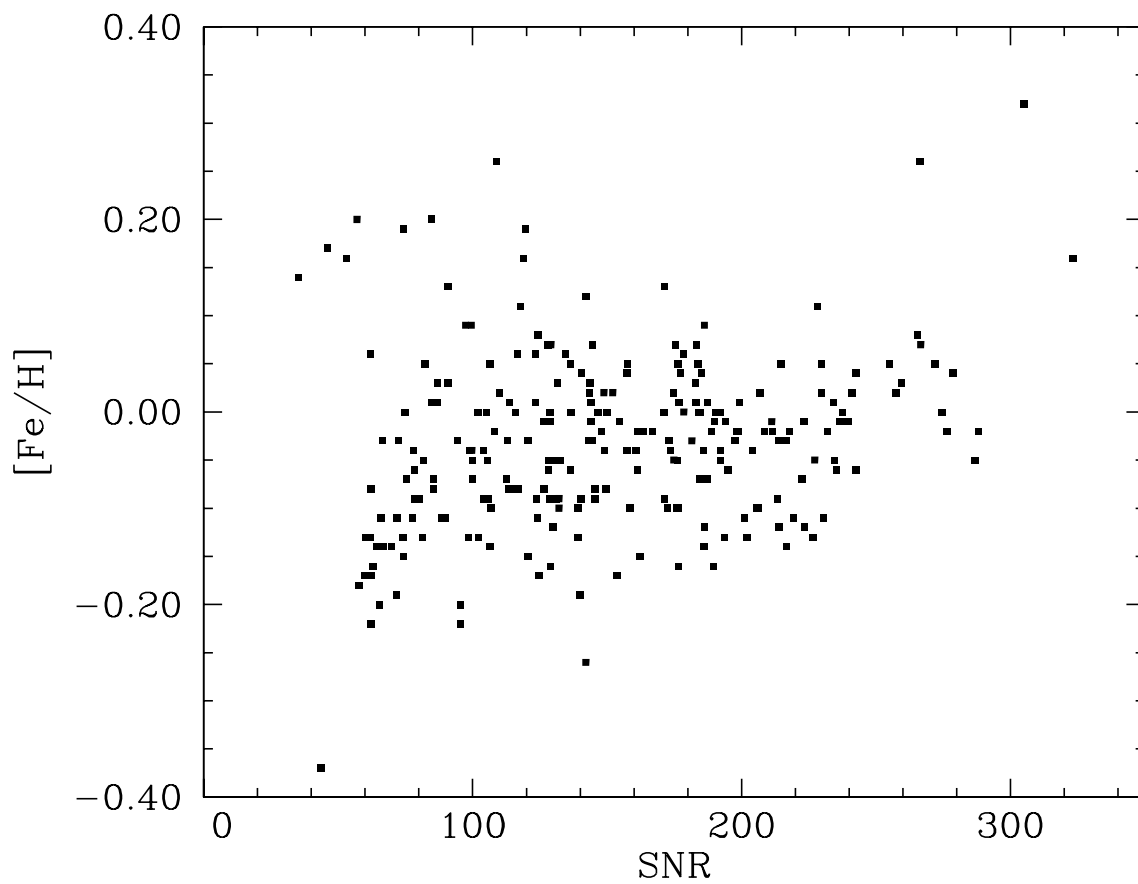


FIG. 2.— For 247 single, probable member stars in NGC 6819, the median iron abundance relative to solar is shown as a function of the spectrum SNR.

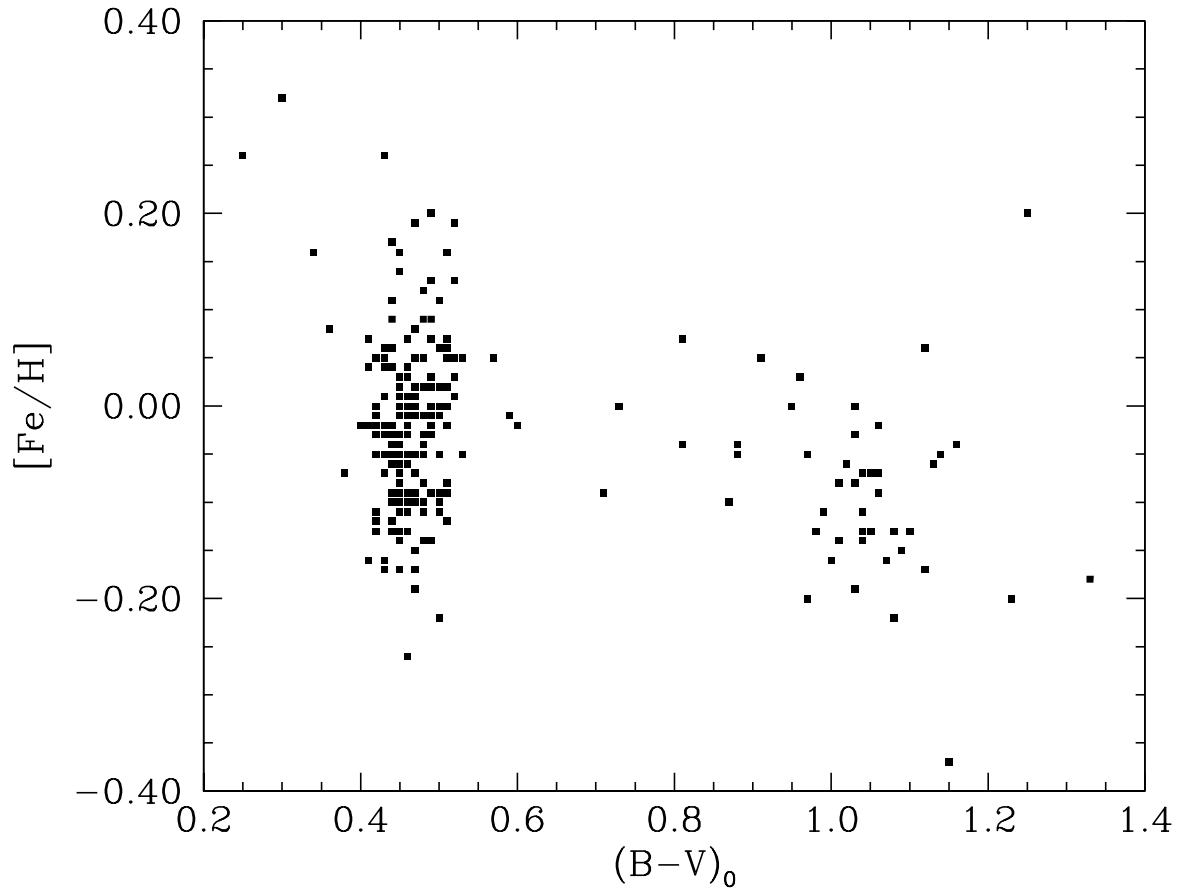


FIG. 3.— For 247 single, probable member stars in NGC 6819, median iron abundances relative to solar is illustrated as a function of reddening-corrected color, $(B-V)_0$.

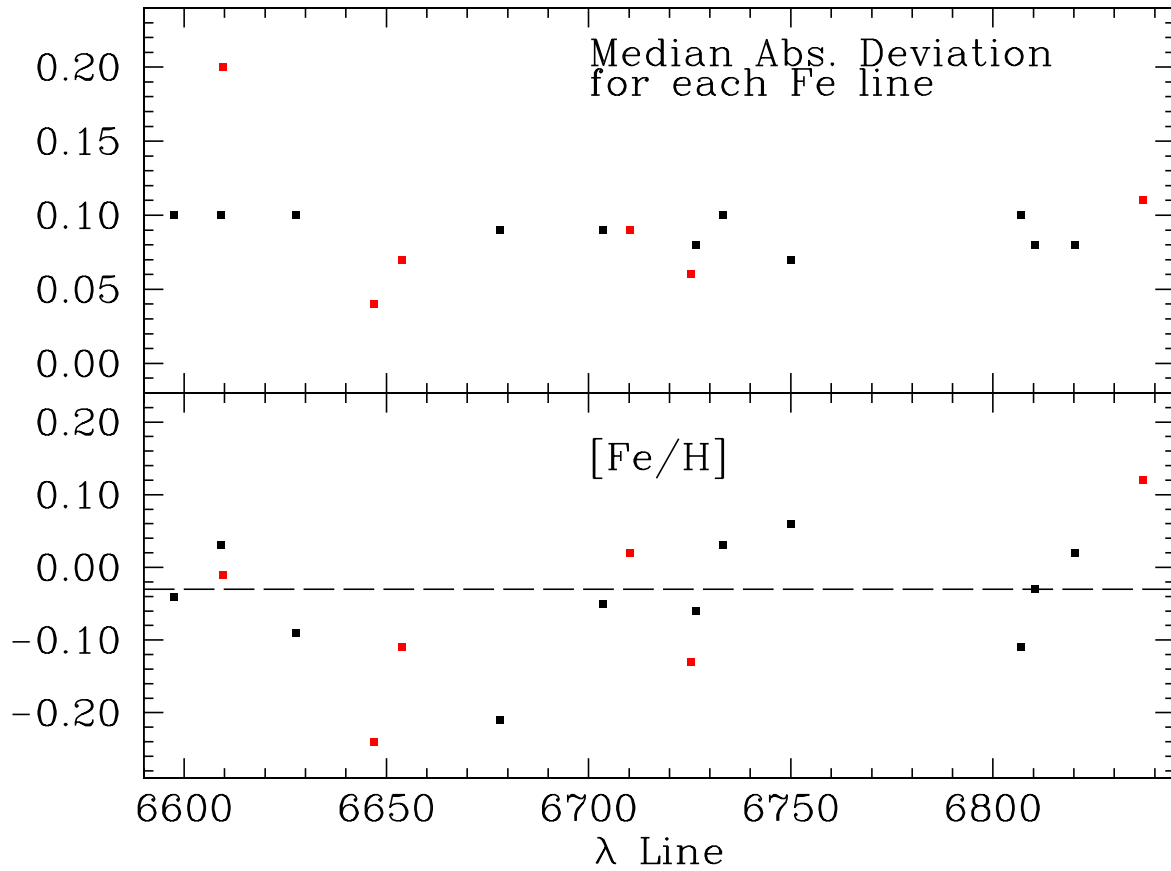


FIG. 4.— For single, probable member stars, the median abundance is shown for each of the 17 iron lines used, plotted as a function of wavelength expressed in Å. The upper panel shows the median absolute deviation of values about each line’s median value. Values denoted by red symbols indicate lines for which only giant stars contribute to the median abundance value. In the bottom panel, the dashed horizontal line denotes the cluster [Fe/H] value of -0.03.

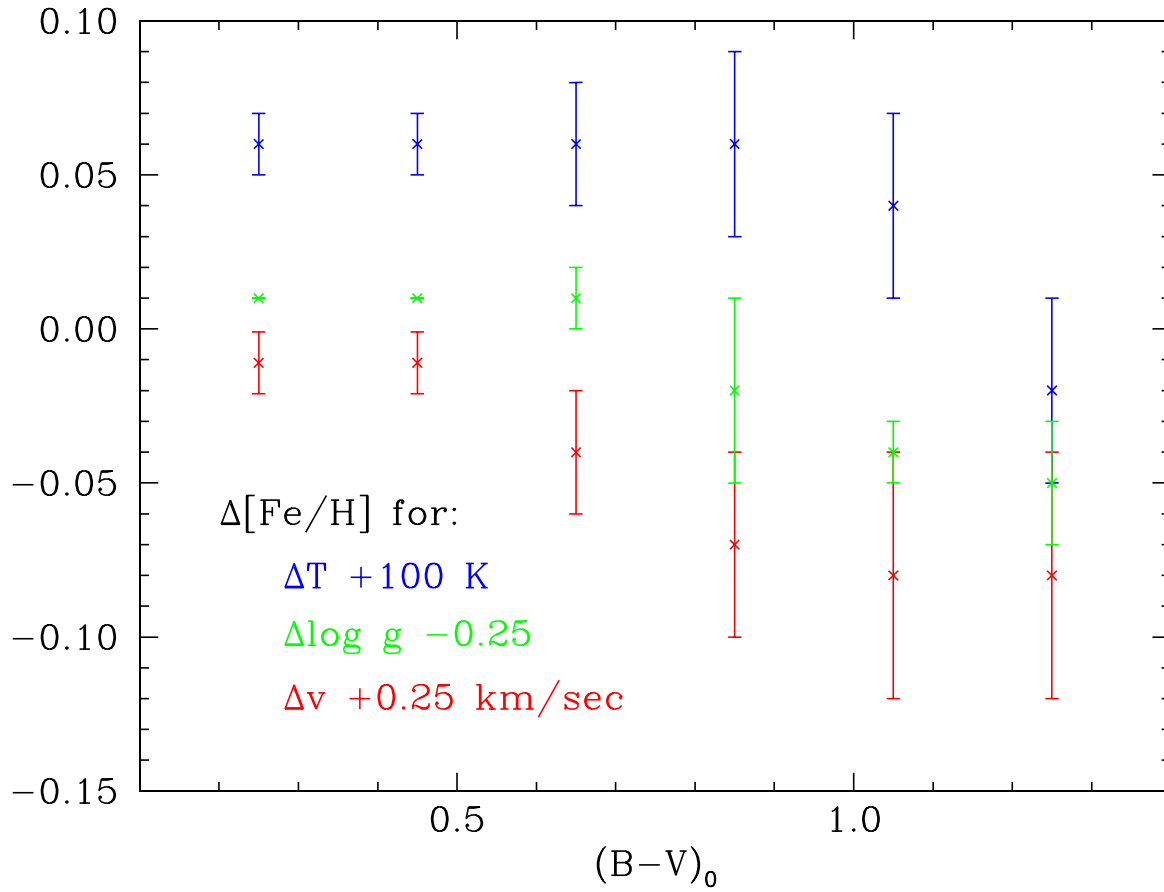


FIG. 5.— Median values of $\Delta[\text{Fe}/\text{H}]$ for stars in unreddened color bins 0.2 mag wide illustrate the effects of increasing the model atmosphere temperature by 100 K (blue filled squares), of increasing the microturbulent velocity parameter by 0.25 km/sec (red cross symbols) and lowering the surface gravity parameter, $\log g$ by 0.25 (green open triangles).

Table 1. Stellar Parameters for NGC 6819 Sample

| WOCS ID | Platais ID | Membr.Prob. | $B - V$ | $E(B - V)$ | Num.Sources | T_{eff} | $\log g$ | V_i | SNR | V_{rot} | $\sigma_{V_{rot}}$ | V_{rad} | $\sigma_{V_{rad}}$ | Comment |
|---------|------------|-------------|---------|------------|-------------|-----------|----------|-------|-----|-----------|--------------------|-----------|--------------------|---------|
| 1002 | 629109 | 99 | 1.558 | 0.167 | 2 | 4136 | 1.52 | 1.70 | 57 | 10.3 | 0.5 | 1.6 | 1.3 | ... |
| 1004 | 651096 | 99 | 1.382 | 0.153 | 2 | 4393 | 1.95 | 1.61 | 66 | 7.1 | 0.2 | 2.0 | 0.9 | ... |
| 1007 | 735344 | 0 | 1.544 | 0.161 | 2 | 4149 | 1.65 | 1.67 | 53 | 8.1 | 0.4 | -1.7 | 1.3 | ... |
| 1014 | 805161 | 99 | 1.560 | 0.154 | 2 | 4113 | 1.52 | 1.70 | 57 | 4.6 | 0.3 | 1.1 | 1.7 | ... |
| 1016 | 845941 | 99 | 1.745 | 0.145 | 1 | 3797 | 1.09 | 1.78 | 19 | 4.6 | 0.6 | 3.1 | 3.4 | ... |
| 2001 | 650699 | 0 | 1.238 | 0.162 | 3 | 4654 | 2.66 | 1.47 | 72 | 7.2 | 0.2 | 0.2 | 0.7 | ... |
| 2003 | 638506 | 99 | 1.142 | 0.164 | 2 | 4839 | 1.59 | 1.68 | 60 | 6.8 | 0.2 | 3.1 | 0.8 | ... |
| 2004 | 670726 | 99 | 1.324 | 0.160 | 2 | 4500 | 2.22 | 1.56 | 100 | 7.9 | 0.2 | 0.4 | 0.8 | ... |
| 2006 | 687312 | 98 | 1.204 | 0.166 | 3 | 4724 | 2.48 | 1.50 | 72 | 14.2 | 0.4 | 1.0 | 0.8 | ... |
| 2007 | 713501 | 99 | 1.205 | 0.163 | 3 | 4716 | 2.48 | 1.50 | 76 | 5.3 | 0.2 | 3.2 | 0.8 | ... |
| 2012 | 505036 | 98 | 1.197 | 0.151 | 3 | 4709 | 2.48 | 1.50 | 107 | 7.3 | 0.2 | 0.0 | 0.7 | SB1 |
| 2016 | 721388 | 99 | 1.759 | 0.171 | 1 | 3818 | 1.09 | 1.78 | 18 | 31.2 | 7.1 | 9.1 | 4.4 | ... |
| 3001 | 656659 | 99 | 1.169 | 0.166 | 3 | 4790 | 2.78 | 1.44 | 129 | 15.9 | 0.4 | 2.1 | 0.7 | ... |
| 3003 | 651311 | 99 | 1.301 | 0.148 | 2 | 4519 | 1.56 | 1.69 | 44 | 4.1 | 0.2 | 3.5 | 1.4 | ... |
| 3004 | 611400 | 99 | 1.228 | 0.173 | 3 | 4692 | 2.54 | 1.49 | 113 | 7.4 | 0.2 | 1.2 | 0.7 | ... |
| 3005 | 667224 | 99 | 1.234 | 0.165 | 3 | 4666 | 2.48 | 1.50 | 63 | 6.7 | 0.2 | 2.4 | 0.8 | ... |
| 3007 | 730339 | 99 | 1.203 | 0.157 | 3 | 4709 | 2.48 | 1.50 | 74 | 6.2 | 0.2 | 2.3 | 0.7 | ... |
| 3009 | 758213 | 99 | 1.202 | 0.163 | 2 | 4722 | 2.39 | 1.52 | 139 | 7.3 | 0.2 | 2.5 | 0.8 | ... |
| 3021 | 896096 | 21 | 1.138 | 0.163 | 1 | 4845 | 2.45 | 1.51 | 98 | 8.3 | 0.2 | 1.3 | 0.7 | ... |
| 4001 | 648574 | 98 | 1.189 | 0.159 | 4 | 4739 | 2.91 | 1.42 | 85 | 8.1 | 0.2 | 1.7 | 0.8 | ... |

Note. — Units for velocities and associated errors are $\text{km}\cdot\text{s}^{-1}$, $\text{cm}\cdot\text{s}^{-2}$ for surface gravity, Kelvin for T_{eff} .

Table 2. Lines used for Abundance Analysis

| Wavelength | Element | EP | $\log gf$ |
|------------|---------|------|-----------|
| 6597.56 | Fe | 4.80 | -1.04 |
| 6609.11 | Fe | 2.56 | -2.71 |
| 6609.68 | Fe | 0.99 | -5.24 |
| 6627.54 | Fe | 4.55 | -1.57 |
| 6646.93 | Fe | 2.61 | -3.87 |
| 6653.91 | Fe | 4.15 | -2.44 |
| 6677.99 | Fe | 2.56 | -1.50 |
| 6703.57 | Fe | 2.76 | -3.02 |
| 6710.32 | Fe | 1.49 | -4.77 |
| 6725.36 | Fe | 4.10 | -2.35 |
| 6726.67 | Fe | 4.61 | -1.16 |
| 6733.15 | Fe | 4.64 | -1.62 |
| 6750.15 | Fe | 2.42 | -2.80 |
| 6806.86 | Fe | 2.73 | -3.14 |
| 6810.27 | Fe | 4.61 | -1.08 |
| 6820.37 | Fe | 4.64 | -1.20 |
| 6837.01 | Fe | 4.59 | -1.82 |
| 6717.68 | Ca | 2.71 | -0.22 |
| 6721.85 | Si | 5.86 | -1.09 |
| 6643.63 | Ni | 1.68 | -1.83 |
| 6767.77 | Ni | 1.83 | -2.23 |
| 6772.31 | Ni | 3.66 | -1.00 |

Note. — Wavelengths are expressed in Å units, excitation potentials in electron volts. All abundances refer to neutral atoms.

Table 3. Abundances for Individual Stars in NGC 6819 Sample

| WOCS ID | [Fe/H] | MAD | N(Fe) | [Ca/H] | [Si/H] | [Ni/H] | Note |
|---------|--------|------|-------|--------|--------|--------|-------|
| 1002 | -0.31 | 0.22 | 15 | ... | 0.17 | -0.34 | NM/BC |
| 1004 | -0.20 | 0.09 | 16 | ... | 0.05 | -0.06 | |
| 1007 | -0.21 | 0.13 | 16 | ... | 0.29 | -0.03 | NM/BC |
| 1014 | -0.28 | 0.20 | 16 | ... | 0.10 | -0.10 | NM/BC |
| 1016 | -0.75 | 0.61 | 16 | -0.67 | ... | -1.47 | NM/BC |
| 2001 | -0.07 | 0.12 | 16 | ... | 0.12 | -0.02 | NM/BC |
| 2003 | -0.13 | 0.12 | 16 | 0.53 | -0.05 | -0.14 | |
| 2004 | -0.04 | 0.10 | 16 | ... | 0.23 | 0.02 | |
| 2006 | -0.11 | 0.05 | 16 | 0.20 | 0.05 | 0.04 | |
| 2007 | -0.07 | 0.11 | 15 | 0.15 | 0.07 | 0.11 | |
| 2012 | -0.13 | 0.07 | 16 | 0.19 | 0.06 | -0.04 | NM/BC |
| 2016 | -0.30 | 1.04 | 6 | ... | ... | -1.58 | NM/BC |
| 3001 | -0.16 | 0.09 | 16 | 0.18 | -0.04 | -0.19 | |
| 3003 | -0.37 | 0.10 | 15 | -1.99 | -0.21 | -0.34 | |
| 3004 | -0.07 | 0.09 | 16 | ... | 0.12 | 0.01 | |
| 3005 | -0.16 | 0.07 | 16 | 0.14 | 0.03 | -0.07 | |
| 3007 | -0.13 | 0.08 | 15 | 0.22 | -0.01 | 0.02 | |
| 3009 | -0.13 | 0.12 | 16 | 0.26 | 0.09 | 0.02 | |
| 3021 | 0.00 | 0.11 | 14 | 0.33 | 0.03 | 0.02 | NM/BC |
| 4001 | -0.08 | 0.07 | 15 | 0.15 | 0.13 | 0.05 | |